AIChE WILEY InterScience DISCOVER SOMETHING GREAT

SEPARATIONS

Optimal Design of Simulated Moving-Bed Processes under Flow Rate Uncertainty

José P. B. Mota, João M. M. Araújo, and Rui. C. R. Rodrigues
Requimte/CQFB, Departamento de Química, Faculdade de Ciências e Tecnologia, Universidade Nova de Lisboa, 2829-516 Caparica, Portugal

DOI 10.1002/aic.11281
Published online August 24, 2007 in Wiley InterScience (www.interscience.wiley.com).

A general procedure for robust design of simulated moving-bed (SMB) processes under flow rate uncertainty is presented. The best solution is chosen only among candidate solutions that are robust feasible, that is, remain feasible for all flow rate perturbations from the uncertainty set. This gives rise to a robust approach to optimal SMB design in which the nominal problem is replaced by a worst case problem. Computational tractability is ensured by formulating the robust problem with only the vertices of the uncertainty region that most adversely affect the raffinate and extract purities. The nominal optimization problem and its robust counterpart are formulated with a single-column analog model, and a full-discretization approach for steady periodic dynamics. The resulting nonlinear programming problems are solved by an efficient interior-point solver. The procedure is successfully employed to find robust operating conditions for the linear separation of two nucleosides by standard SMB, asynchronous port switching (Varicol), and cyclic flow rate modulation (PowerFeed). Our results show that PowerFeed is the most efficient operating scheme for the separation under study, although Varicol also clearly outperforms the standard SMB process. However, it is also shown that Varicol productivity is the least affected when the process is rendered robust, whereas that of PowerFeed is the most penalized. © 2007 American Institute of Chemical Engineers *AIChE J,* 53: 2630–2642, 2007

Keywords: simulated moving bed, Varicol, PowerFeed, robust optimization, flow rate uncertainty

Introduction

The simulated moving-bed (SMB) technology is a multicolumn adsorptive separation process that increases throughput, purity and yield relative to classical preparative chromatography.[1–3] The SMB process is shown in Figure 1, and was originally devised as a practical implementation of the true moving-bed process, where the adsorbent and the mobile phase move countercurrently.[4] However, contrary to a true countercurrent process, the SMB reaches a cyclic steady state (CSS), where the internal concentration profiles move in the direction of fluid flow and the outlet compositions are time periodic. Details of arranging commercially available two-position and multiposition valves for the operation of the SMB process have been thoroughly reviewed in a recent publication.[5] The SMB was initially developed for hydrocarbon and sugar separations, but is now being increasingly applied in the pharmaceutical, fine chemistry, and biotechnology industries, at all production scales.[6]

Uncertainties in isotherm parameters, band broadening, pump stability and calibration, temperature stability, extra-column volumes, and packing reproducibility, are inevitable in every SMB process. This is particularly true in production-scale operation. Although there have been previous studies on the effect of variations in operating and system parameters on SMB performance, only a few of them have addressed the problems of handling parameter uncertainty and robustness of operation.

Storti et al.[7] and Mazzotti et al.[8] were the first to introduce the concept of robustness in optimal SMB design in the

Correspondence concerning this article should be addressed to J. P. B. Mota at pmota@dq.fct.unl.pt.

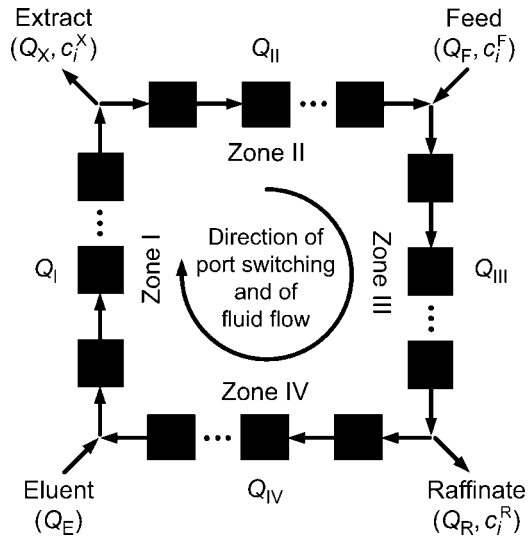

Figure 1. Four-section SMB process.

The system comprises several identical columns which are serially connected in either a closed- or open-loop configuration The column sequence is divided into four zones of constant flow rates by four ports: one for adding fresh desorbent or mobile phase, another one for withdrawing the slow migrating solutes, another one for continuous feeding, and the last one for withdrawing the fast migrating solutes. By periodically moving the input and withdrawal ports in the direction of fluid flow, the countercurrent contact between the stationary and mobile phases is simulated. Desorption or regeneration of the adsorbent take place in zone I. The separation takes place in zones II and III, where the more strongly adsorbed species, or group of species with similarly strong adsorption properties, is conveyed downwards to the extract outlet and the less strongly adsorbed species or group of species upwards to the raffinate outlet, respectively. In the closed-loop configuration, the fast migrating solutes are trapped in zone IV, so as to regenerate the solvent and recycle it back to zone I.

framework of their triangle theory. These authors have nicely shown that the further the operating point is from the boundaries of the complete separation region in the four-dimensional (4-D) space whose coordinates are the m_j flow rate ratios, the more robust the operating conditions are. A quantitative measure of robustness was proposed based on the geometrical location of the operating point in the (m_2, m_3) plane.

More recently, Mun et al.[9] have produced a comprehensive study of how SMB performance is affected by variations in operating and system parameters. Practically every conceivable source of disturbance was taken into consideration and a robust pump configuration for minimizing the effects of pump output deviations was proposed. The authors also extended their standing-wave design method[10,11] to handle robust design. They have shown that even when the worst parameter deviations occur, the desired yield and purity can still be achieved.

In this work we address the issue of robustness in SMB operation, and present a general procedure for robust SMB design under flow rate uncertainty. This is the most difficult operating uncertainty to tackle from a design perspective and one frequently occurring in production-scale operations. Our procedure is not only applicable to the classical SMB process, but also to recently developed nonstandard schemes, such as asynchronous port switching (Varicol)[12,13] and cyclic flow rate modulation (PowerFeed).[14–18] This is a significant achievement. The issue of robustness is particularly important for these newly emerged SMB schemes, because they provide further gains but at the expense of additional complexity and increased sensitivity to operating disturbances.

The article is structured as follows. We start by describing the theoretical framework in which the method is developed, and then present the robust counterpart of the nominal SMB design problem. After briefly describing the adopted solution approach and numerical implementation, the method is validated and its computational tractability demonstrated using the linear separation of two nucleosides by reversed phase as model system. The procedure is successfully employed to find robust operating conditions for standard SMB, Varicol, and PowerFeed schemes. We end with some brief conclusions and perspectives for future work.

Robust Approach to Optimal SMB Design

It is assumed that the experimental realization of the zone flow rates, Q_j (j = I, ..., IV), is subject to an error, or uncertainty, that is bounded by a maximum relative deviation δ, from their nominal values Q_j^*:

$$(1-\delta)Q_j^* \le Q_j \le (1+\delta)Q_j^* \tag{1}$$

In the absence of uncertainty ($\delta = 0$, $Q_j = Q_j^*$), the mathematical programming problem for optimal SMB design can be formulated as follows

$$\max_{\tau, N_j, Q_j} f_{\text{obj}}(\overline{Q}_F, \overline{Q}_E) \tag{2}$$

$$\text{s.t.} \quad y = h^{\text{CSS}}(\tau, N_j, Q_j) \tag{3}$$

$$g(\tau, N_j, Q_j, y) \ge 0 \tag{4}$$

where τ, N_j, and Q_j are the set of design or decision variables, f_{obj} is an objective function to be maximized, which has productivity

$$\overline{Q}_F = \frac{1}{\tau}\int_t^{t+\tau} (Q_{III} - Q_{II})\mathrm{d}t \tag{5}$$

and/or solvent consumption

$$\overline{Q}_E = \frac{1}{\tau}\int_t^{t+\tau} (Q_I - Q_{IV})\mathrm{d}t \tag{6}$$

as arguments, y is the steady periodic solution (concentration profiles) of the chromatographic model (defined by the set of equality constraints h^{CSS}), and g is a set of inequality constraints. These constraints include product quality requirements (purity and recovery), and physical (e.g. column dimensions), and operating restrictions (e.g. pressure drop). Note that when the flow rates are periodically varied over time, the values of Q_F and Q_R must be averaged over a switching interval to determine the relevant values of productivity and eluent consumption.

Equations 2–4 correspond to the simplest problem formulation in terms of design variables, since particle size and column dimensions are excluded from the decision set as

being nonessential to the present discussion. Note, however, that the N_j's are part of the decision variables to allow the optimization of the column configuration or port switching, as is the case for Varicol operation. The most common problem is the maximization of productivity or feed throughput, that is $f_{obj} = \overline{Q}_F$, but other feasible choices exist, such as e.g. the minimization of $\overline{Q}_E$ for a given value of $\overline{Q}_F$.

For convenience the set of inequality constraints g is split into two subsets g_1 and g_2, one dealing specifically with operational feasibility and restrictions,

$$g_1(Q_j) = \left\{ \begin{array}{c} Q_{max} - Q_I \\ Q_{max} - Q_{III} \\ Q_E = Q_I - Q_{IV} \\ Q_X = Q_I - Q_{II} \\ Q_F = Q_{III} - Q_{II} \\ Q_R = Q_{III} - Q_{IV} \end{array} \right\} \geq 0 \tag{7}$$

and the other imposing requirements on product quality

$$g_2(\tau, N_j, Q_j, y) = \left\{ \begin{array}{c} P_R(\tau, N_j, Q_j, y) - P_R^{min} \\ P_X(\tau, N_j, Q_j, y) - P_X^{min} \end{array} \right\} \geq 0 \tag{8}$$

Here P_R and P_X are the raffinate and extract purities, respectively, and P_R^{min} and P_X^{min} are their minimal acceptable values. Parameter Q_{max} is the largest allowed operating flow rate in zones I and III. The value of Q_{max} is constrained by either the capacity of the installed pumps, or the efficiency and functionality of the stationary phase, which in most cases is only guaranteed up to a maximum interstitial fluid velocity, or by the pressure drop in the plant. Both sets of constraints are assumed to be "hard," that is, violations of any of them, even small ones, cannot be tolerated. The only allowed exceptions are the first two constraints of g_1, which can be violated when Q_{max} is dictated by the capacity of the installed pumps.

In PowerFeed operation some, or all, of the flow rates are changed from continuous constant flow to τ-periodic flow, while still satisfying at every instant the global constraint $Q_E + Q_F = Q_X + Q_R$. The τ-periodic flow rate modulations considered in this work are piecewise constant. In practice, the switching interval is divided into n_Q subintervals of equal length and the flow rates remain constant over each subinterval before jumping discretely to different values over the next subinterval. Thus, in this work each Q_j is either a scalar or a vector of length n_Q. In the latter case, the g_1 set of constraints must be separately applied to each subinterval of the flow-rate modulation.

The numerical experiments supporting this work show that even slight perturbations of the nominal values of the flow rates may result in a severe infeasibility of the optimal solution for the SMB design problem. When satisfying the feasibility constraints is important, and often this is the case for the purity requirements expressed by g_2, such "nonrobustness" with respect to constraint violations can make the nominal solution misleading or of little use. To avoid this, the best solution should be chosen only among those "immunized" against flow rate uncertainty. By this we mean that the candidate solutions should be robust feasible, that is, remain feasible for all flow rate perturbations from the uncertainty set defined by Eq. 1. This observation is the basis for the proposed robust approach to optimal SMB design where the nominal problem is replaced by a "worst case" problem.[19–22]

What is claimed in the present work is that the optimal solution (τ, N_j and Q_j^*) of the SMB design problem, when subject to the flow rate uncertainty given by Eq. 1, can be obtained from its robust counterpart (RC), which can be written as

$$\max_{\tau, N_j, Q_j^*} f_{obj}(\overline{Q}_F^*, \overline{Q}_E^*) \tag{9}$$

$$\text{s.t.} \left\{ \begin{array}{l} Q_j^- = Q_j^-(\delta, Q_j^*) \\ Q_j^+ = Q_j^+(\delta, Q_j^*) \end{array} \right. \tag{10}$$

$$y^{\pm} = h^{CSS}(\tau, N_j, Q^{\pm}) \tag{11}$$

$$g_1'(Q_j^*) = \left\{ \begin{array}{c} Q_{max} - Q_I^* \\ Q_{max} - Q_{III}^* \\ (1-\delta)Q_I^* - (1+\delta)Q_{IV}^* \\ (1-\delta)Q_I^* - (1+\delta)Q_{II}^* \\ (1-\delta)Q_{III}^* - (1+\delta)Q_{II}^* \\ (1-\delta)Q_{III}^* - (1+\delta)Q_{IV}^* \end{array} \right\} \geq 0 \tag{12}$$

$$g_2(\tau, N_j, Q^+, y^+) \geq 0, \quad g_2(\tau, N_j, Q^-, y^-) \geq 0 \tag{13}$$

Here $Q^- \equiv [Q_I^-, \ldots, Q_{IV}^-]$ and $Q^+ \equiv [Q_I{}^+, \ldots, Q_{IV}{}^+]$ are the two perturbations of the optimal flow rates that define the lowest and left-most vertices, respectively, of the 4-D uncertainty region projected onto the (P_R, P_X) plane. This is depicted in Figure 2 for the two different geometrical shapes of the projected region that have been identified in this work. Q^- and Q^+ perturbations are, thus, responsible for the worst violations of the g_2 constraints. In Eq. 12, the nominal g_1 constraints have been adjusted in order to immunize the robust solution against the worst case deviations. If the violation of the first two g_1 constraints cannot be tolerated then the first two entries of g_1' should read $Q_{max} - (1 + \delta)\, Q_I^*$ and $Q_{max} - (1 + \delta)\, Q_{III}^*$.

In principle one should look for Q^- and Q^+ among the $2^4 = 16$ vertices of the edges that bound the 4-D uncertainty region, but fortunately most of those vertices can be excluded in advance from the search. For example, we have determined that for the numerical experiments reported here there are only two likely candidates for the lowest vertex, where P_X is decreased most

$$Q^- = [(1+\delta)Q_I^*, (1-\delta)Q_{II}^*, (1-\delta)Q_{III}^*, (1+\delta)Q_{IV}^*] \tag{14}$$

$$Q^- = [(1+\delta)Q_I^*, (1-\delta)Q_{II}^*, (1+\delta)Q_{III}^*, (1+\delta)Q_{IV}^*] \tag{15}$$

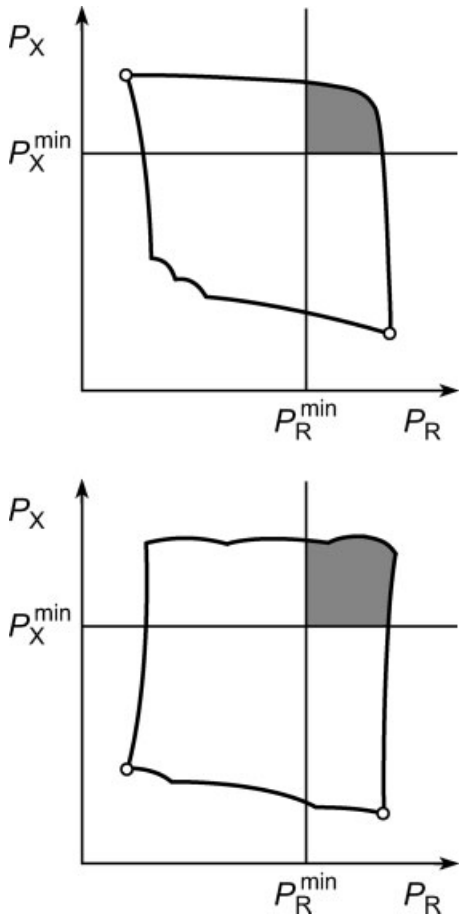

Figure 2. Shapes of the domain obtained by projecting the flow rate uncertainties defined by Eq. 1 onto the (P_R, P_X) plane.

The shaded area represents the feasible region of the domain. The top graph is representative of the case where the lowest and left-most vertices of the domain are obtained for $Q^{\pm} = [(1 \mp \delta)Q_I^*, (1 \pm \delta)Q_{II}^*, (1 \pm \delta)Q_{III}^*, (1 \mp \delta)Q_{IV}^*]$, whereas the bottom graph is qualitatively obtained when the worst-case perturbations are $Q^{\pm} = [(1 \mp \delta)Q_I^*, (1 - \delta)Q_{II}^*, (1 + \delta)Q_{III}^*, (1 \mp \delta)Q_{IV}^*]$.

and two others for the left-most vertex, where P_R is reduced most

$$Q^+ = [(1-\delta)Q_I^*, (1+\delta)Q_{II}^*, (1+\delta)Q_{III}^*, (1-\delta)Q_{IV}^*] \quad (16)$$

$$Q^+ = [(1-\delta)Q_I^*, (1-\delta)Q_{II}^*, (1+\delta)Q_{III}^*, (1-\delta)Q_{IV}^*] \quad (17)$$

These two extreme cases are depicted in Figure 2. The top graph is qualitatively obtained when the worst-case vertices are defined by Eqs. 14 and 16, whereas the bottom graph is representative of the case given by Eqs. 15 and 17. In the absence of further knowledge, the RC problem must thus be solved with two candidate perturbations for Q^- and two others for Q^+ and, consequently, four components in Eqs. 10, 11 and 13. However, if one is solving a series of similar problems, such as when generating a Pareto curve, the worst-case perturbations can be predetermined in advance, so that the series of RC problems can be solved with a single perturbation for Q^- and another one for Q^+. This is elaborated in more detail following.

It is worth noting that none of the perturbations defined by Eqs. 14–17 is

$$[(1-\delta)Q_I^*, (1-\delta)Q_{II}^*, (1+\delta)Q_{III}^*, (1+\delta)Q_{IV}^*] \quad (18)$$

which reduces the eluent flow rate to the lower edge of its confidence interval, while increasing the feed flow rate to its upper edge. In reality, this perturbation is the worst one only when product quality is globally assessed by the purity index, $PI = (P_X + P_R)/2 \geq PI^{min}$. This quality requirement is clearly less restrictive than the two g_2 constraints applied simultaneously.

It should be pointed out that there is an increase in complexity while moving from the nominal problem to its robust counterpart, because the latter works simultaneously with more than one instance of the chromatographic model. However, we shall demonstrate that the RC problem remains computationally tractable if the right solution approach and optimization solver are employed. In fact, the numerical experiments reported in this work show that the CPU time required to obtain a robust solution on standard computing hardware is of the order of minutes.

Computational Implementation

We employ a recently developed[23] compact representation of the SMB process as a convenient framework for implementing an efficient solution method for the nominal optimization problem and its robust counterpart. This formulation is particularly useful for the optimization of Varicol operation since it encompasses a whole class of physically realizable asynchronous port switching schemes that are univocally specified by only four rational numbers $N_I, \ldots, N_{IV}$, which define the average number of columns over a switching interval in each zone of the SMB unit. If the N_j's are all integers then the standard SMB process with N_j columns in zone j is obtained. This formulation has the advantages of substantially reducing the dimension of the searchable Varicol space and eliminating the integer nature of the optimization problem.[23–25]

Part of the solution strategy relies on the direct calculation of the steady periodic solution for a single-column model that replicates the cyclic steady state of the equivalent multi-column process.[26,27] For this purpose, a full-discretization method is applied to the single-column model in which the time coordinate is discretized over a full cycle ($N\tau$ time units), and a periodic condition is directly imposed. The computational domain and governing equations are given in Figure 3, together with a diagram of the single-column model.

Discretization is handled via collocation, using 10 cubic Hermite elements for the spatial domain and $10N$ Radau elements (with two interior points) for the time domain. The latter type of collocation elements is especially suitable for handling process dynamics with frequent discontinuities in time.[28] Both the port configuration and the flow rates remain constant over each Radau element, but are allowed to change discretely to different values across elements. This means that the optimized value for each N_j is obtained with an accuracy

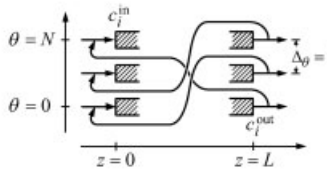

Dimensionless time coordinate:

$$\theta = t/\tau, \quad \theta' = \theta \bmod 1, \quad \overline{\theta} = \theta \bmod N, \quad \theta_j = \sum_{k=j}^{4} N_k, \ j = 1, ..., 4$$

Computational domain:

$$\Omega = \Omega_z \times \Omega_\theta, \quad \Omega_\theta = [0, N], \ \ \Omega_z = [0, L]$$

Formulate chromatographic column model with cyclic condition:

$$c_i(z, N) = c_i(z, 0), \ \ q_i(z, N) = q_i(z, 0), \ \ \forall z \in \Omega_z$$

Condition for simulated countercurrent (SCC) flow:

$$c_i(z, \overline{\theta+1}) = c_i(z, \theta), \ \ q_i(z, \overline{\theta+1}) = q_i(z, \theta), \ \ \forall z \times \theta \in \Omega$$

Inlet node balance with embedded SCC condition:

$$\begin{aligned} Q_{III}(\theta')\, c_i^{in}(\theta) &= Q_{II}(\theta')\, c_i^{out}(\overline{\theta+1}) + \\ &\quad + [Q_{III}(\theta') - Q_{II}(\theta')]\, c_i^{F}(\theta'), && \theta_3 - 1 < \theta < \theta_3 \\ Q_I(\theta')\, c_i^{in}(\theta) &= Q_{IV}(\theta')\, c_i^{out}(\overline{\theta+1}), && \theta_1 - 1 < \theta < \theta_1 \\ c_i^{in}(\theta) &= c_i^{out}(\overline{\theta+1})', && \text{otherwise} \end{aligned}$$

Temporal flow-rate profile in the column:

$$Q(\theta) = Q_j(\theta') \quad \text{for} \quad \theta_{j+1} < \theta < \theta_j, \ \ j = 1, ..., 4$$

Raffinate withdrawal period: $\Omega_R = [\theta_4, \theta_4 + 1]$

$$c_i^{R}(\theta) = \frac{Q(\theta)\, c_i^{out}(\theta) + [Q_{III}(\theta') - Q(\theta)]\, c_i^{F}(\theta')}{Q_{III}(\theta')}$$

Extract withdrawal period: $\Omega_X = \begin{cases} [\theta_2, \theta_2 + 1] & N_I \geq 1 \\ [0, \theta_2 + 1 - \theta_1] \cup [\theta_2, \theta_1] & N_I < 1 \end{cases}$

$$c_i^{X}(\theta) = Q(\theta)\, c_i^{out}(\theta) \,/\, Q_I(\theta')$$

Purities ($Q_X = Q_I - Q_{II}$, $Q_R = Q_{III} - Q_{IV}$):

$$P_X = \frac{\int_{\Omega_X} Q_X(\theta')\, c_2^{X}\, d\theta}{\int_{\Omega_X} Q_X(\theta')\, (c_1^{X} + c_2^{X})\, d\theta}, \quad P_R = \frac{\int_{\Omega_R} Q_R(\theta')\, c_1^{R}\, d\theta}{\int_{\Omega_R} Q_R(\theta')\, (c_1^{R} + c_2^{R})\, d\theta}$$

Figure 3. Main governing equations for single-column model with "recycle lead" that replicates the cyclic steady state of the equivalent multicolumn process.

The equations for the chromatographic column model are not listed for the sake of brevity.

of ca. $\pm 0.5/n_\tau$, where $n_\tau = 10$ is the number of Radau elements employed per switching interval. This is also the highest resolution at which the flow rate modulation for PowerFeed operation can be discretized. This is perfectly adequate for virtually every practical application, since higher resolutions have little impact on the objective function.

As proposed by Kawajiri and Biegler,[28,29] the nonlinear programming problem obtained after discretization is formulated in AMPL,[30] and solved using IPOPT 3.2.3.[31] This solution strategy has been previously employed with success by our group on a broad class of SMB problems.[32–34] IPOPT implements a primal-dual interior-point method, and uses line searches based on filter methods. It directly exploits first and second derivative (Hessians) information provided by AMPL via automatic differentiation.

Varicol optimization is handled slightly differently from described above. The optimization problem is decomposed into an outer problem with the N_j's as the only decision variables, and an inner problem encompassing all other decision variables, i.e.

$$\max_{\tau, N_j, Q_j} f_{obj}(\overline{Q}_F, \overline{Q}_E) \rightarrow \max_{N_j} \{ \max_{\tau, Q_j} f_{obj}(\overline{Q}_F, \overline{Q}_E), \text{fixed } N_j \} \quad (19)$$

Note that only three of the four zone lengths are decision variables, since they must obey the constraint $\Sigma\ N_j = N$, where N is the total number of columns. Furthermore, they must also satisfy the constraints for physical realizability[23]

$$N_j + N_{j+1} \geq 1 \ (j = I, \ldots, III), \quad N_I + N_{IV} \geq 1 \quad (20)$$

The outer problem is handled by the SQP solver FFSQP 3.7,[35] which in turn calls IPOPT to solve the inner problem for each trial port configuration generated. This is outlined in Figure 4. The gradient of the objective function with respect to the decision variables is computed by first-order backward or forward differencing with a perturbation factor $\Delta N_j = 1/n_\tau$ (i.e. each N_j is decreased or increased by the equivalent to one Radau element). The gradients of the constraints in Eq. 20, on the other hand, are computed analytically.

Results and Discussion

The linear separation of two nucleosides (uridine and guanosine) on reversed phase SOURCE 30RPC (GE Healthcare Amersham Biosciences, Uppsala, Sweden) is used here as a model system to validate the proposed procedure. The mobile phase is 5% (v/v) ethanol in water, which has previously been found to give adequate retention and separation factors.[36] Column characterization and adsorption parameters, which were taken from our previous studies,[32,33] are listed in Table 1.

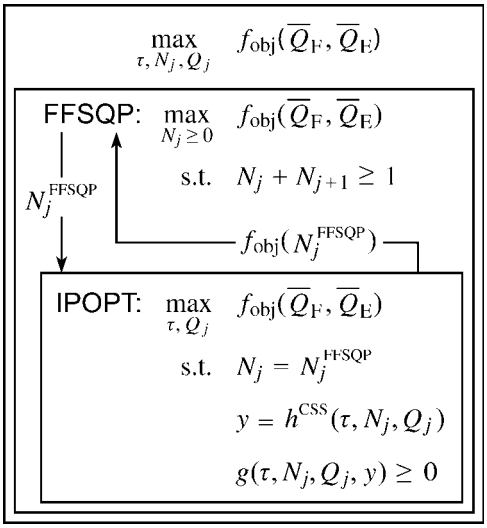

Figure 4. Outline of the solution procedure for Varicol optimization.

Table 1. Column Characterization and Adsorption Parameters

L (cm)	d_c (cm)	V_e (cm^3)	ε
6.0	1.0	0.143	0.265
	K	Pe	αL (s)
Uridine	1.197	442	0.029
Guanosine	1.907	437	0.034

Band broadening is taken into account through a simplified van Deemter curve for each solute

$$\frac{H_i}{2} = \frac{L}{\mathrm{Pe}_i} + \alpha_i v \tag{21}$$

where H_i is the plate height, Pe_i is the Péclet number, and α_i is the slope of the linear dependence with interstitial velocity. Extra-column volume V_e, is modeled as a perfectly mixed cell placed between each column outlet and the adjacent withdrawal port

$$V_e \frac{\mathrm{d}c_i^{\mathrm{out}}}{\mathrm{d}t} = Q(c_i|_{z=L} - c_i^{\mathrm{out}}) \tag{22}$$

where $c_i|_{z=L}$ is the outlet concentration of solute i.

The parameter values for the optimization constraints are $Q_{\max} = 25$ ml/min, and $P_R^{\min} = P_X^{\min} = 0.98$. The reference system is a four-column unit ($N = 4$), which can be operated as a conventional SMB process, in Varicol configuration, or under PowerFeed mode. For each of these operating schemes, the proposed robust optimization procedure is employed to find optimal operating conditions that maximize the feed throughput $f_{\mathrm{obj}} = \overline{Q}_F$, subject to an uncertainty in the flow rates of $\pm 2.5\%$.

The optimizations were carried out on a Pentium IV 1.7 GHz Windows XP machine with 512 MB of RAM. The obtained results are summarized in Table 2. Each pair of nominal/robust solutions for the different operating schemes is discussed in turn and is preceded by a short description of how the solutions were obtained in practice and the required computational effort in terms of CPU time.

Standard SMB operation

Prior to determining the optimal value of the decision variables for the standard SMB scheme, its CSS solution (y in Eq. 3) was computed for an initial estimate of τ and Q_j^* by solving the nominal problem with no objective function and no inequality constraints; in this case, IPOPT's goal is to simply find the solution satisfying Eq. 3. This took 1.3 CPU s on our machine. From this initial state, the optimal solution of the nominal problem (first row of Table 2) was found in 22.8 CPU s and required 19 IPOPT iterations. This problem consists of 5,293 nonlinear variables, 5,288 equality constraints, and 24 inequality constraints. This solution was, subsequently, rendered robust (second row of Table 2) by solving the RC problem in 2.00 CPU min and 16 IPOPT iterations. In the absence of prior knowledge, the four likely candidates for the worst-case perturbations (cf. Eqs. 14–17) had to be considered in Eqs. 11 and 13. This larger RC problem consists of 21,133 nonlinear variables, and 21,164 constraints (28 linear constraints). However, and as expected, the analysis of the residuals of g_2 for the optimal robust solution showed that only two of its components were active. These were for Q^- and Q^+ given by Eqs. 14 and 16, respectively. If this was known in advance, the dimension of the RC problem would have been reduced to 10,565 variables and 10,572 constraints, and take less than half the time to solve (47.8 CPU s). These CPU times clearly show that the computational tractability of the method is not an issue, at least for the problem under study.

We now proceed to show that the robust solution remains, as intended, feasible for all flow rate perturbations within the specified uncertainty. Figure 5 shows an histogram of extract and raffinate purities for a factorial perturbation ($3^4 - 1 = 80$ points) of the nominal and robust values of the optimized flow rates for the standard SMB scheme (the first two rows of Table 2). The nominal and robust solutions for the Varicol and PowerFeed schemes were also subject to a similar analysis; the results are in agreement with those reported below, but are not reproduced here for the sake of brevity.

Each factorial analysis consists of all possible combinations of -2.5%, 0% and $+2.5\%$ relative deviations of the four flow rates, and was performed by repeatedly calling IPOPT, with no objective function and no inequality constraints, to find the solution satisfying the CSS problem for each perturbation. Each factorial analysis took ca. 2 min. This is a significant result, since it is possible that the worst-case perturbations be different from those given by Eqs. 14–17 if the purity requirements or isotherm shape are significantly changed. However, given that the factorial analysis can be performed quickly, the trial perturbations can be easily checked for correctness and adjusted if necessary.

The horizontal axis of the histogram plotted in Figure 5 is an array of symbols with the factorial experiments sorting the columns and the individual zone flow rates forming the rows. This way a specific perturbation can be easily identi-

Table 2. Results of Throughput Maximization for Nominal ($\delta = 0$) and robust ($\delta = 0.025$) Optimization Problems

Scheme	δ (%)	τ	Q_I	Q_{II}	Q_{III}	Q_{IV}	Q_F	Q_E/Q_F
SMB	0.0	0.365	25.00	15.90	19.75	13.49	3.86	2.99
	2.5	0.378	25.00	15.82	18.53	12.64	2.71	4.55
PowerFeed	0.0	0.342	25.00	15.99	22.61	15.03	6.63	1.50
	2.5	0.356	25.00	15.98	20.82	13.79	4.84	2.32
Varicol	0.0	0.350	25.00	15.83	22.00	0.273	6.18	4.00
	2.5	0.360	25.00	15.86	20.90	0.194	5.04	4.92

The optimized Varicol configuration is 1.2/1.2/1.6/0.0. Flow rate modulation for PowerFeed scheme is piecewise constant with $n_Q = 5$ subintervals per switching interval. The flow rates are expressed in mL/min and τ in min.

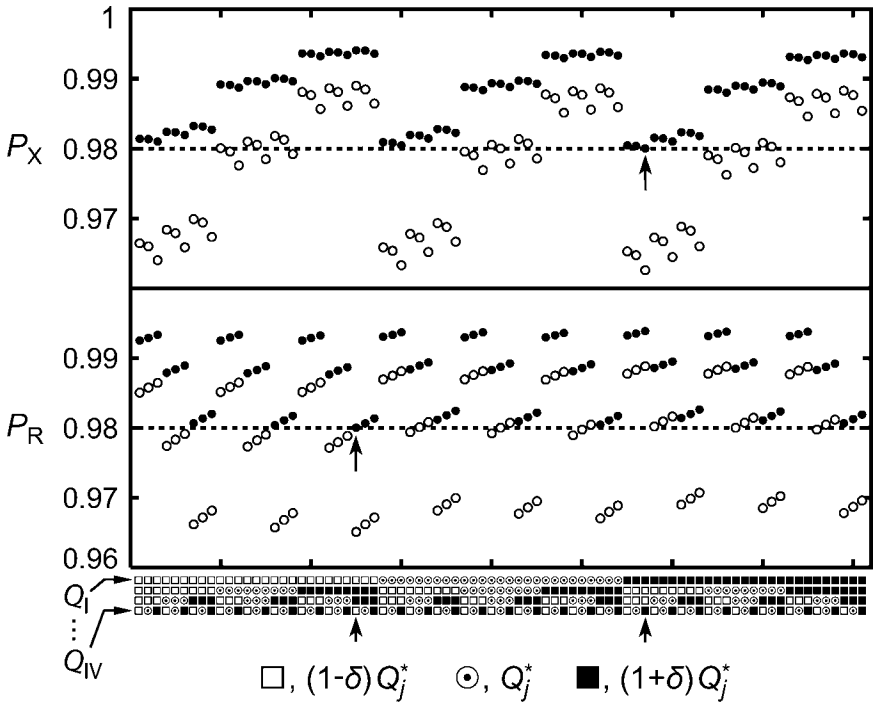

Figure 5. Extract (P_X) and raffinate (P_R) purities for the factorial flow rate perturbation (base solution plus $3^4 - 1 = 80$ perturbations) of the robust (solid circles, $\delta = \pm 2.5\%$) and nominal (open circles, $\delta = 0\%$) optimized solutions for the standard SMB scheme.

The factorial analysis includes all possible combinations of -2.5%, 0% and $+2.5\%$ variations of $Q_I^*, \ldots, Q_{IV}^*$. The vertical arrows point to the perturbations of the robust solution for which $P_X = P_X^{min}$ and $P_R = P_R^{min}$.

fied among the 81 data points. The meaning of each symbol is as follows: "□" is for the lower edge of the confidence interval of Q_j, "⊙" is for no change, and "■" is for the upper edge of its confidence interval. This figure shows that even slight perturbations of the flow rates may result in a severe infeasibility of the optimal solution for the nominal problem; in the severest case the purity drops below 0.965. The robust solution, however, is fully immunized against perturbations in the values of Q_j, as long they stay confined to the specified confidence interval. The worst purity deviations for the standard SMB scheme are obtained for the perturbations given by Eqs. 14 and 16, in agreement with the analysis of the residuals of g_2 for the robust solution.

As expected, robust operation is achieved at the expense of reducing feed throughput and increasing solvent consumption. However, the actual loss in separation performance, 29.8% reduction in Q_F and 52.2% increase in Q_E/Q_F, is much larger than might be anticipated for a confidence interval of only $\pm 2.5\%$. This shows that the optimal conditions for nominal operation are not robust at all, and that the process must be operated rather conservatively in order to withstand even slight disturbances in the flow rates. Still, the robust operating point provided by our approach is optimal, since it is the one that yields the best separation performance for the specified uncertainty.

Figure 5 repays careful study. It provides, in essence, the net effect of disturbing the optimal operating point in the 4-D space whose coordinates are the zone flow rates. Within the scatter of the purity histograms there are easily distinguishable trends, or clusters, that can be associated to specific patterns in the array of symbols, which, in turn, identify the perturbations giving rise to them. If this information is supplemented by plots of the solute concentration profiles for selected flow rate disturbances, as provided in Figure 6, then a better understanding of the influence of each zone flow rate on product purity is obtained. This is discussed next. Figure 6 includes the concentration profiles for the robust optimized solution, those for the two worst-case perturbations, as well as those that delimit the projected uncertainty, both in space and in time.

Extract purity is mostly affected by changes in Q_{II}, because this flow rate directly influences the positioning of the trailing band of the fast-moving solute with respect to the extract port. If Q_{II} is increased, the trailing wave of the fast-moving solute will migrate faster than the extract port and have less chance of getting past it. Inversely, when Q_{II} is lowered the fast-moving solute migrates toward the extract port and contaminates it. Extract purity is also negatively affected, but less severely, when Q_{III} is decreased or Q_{IV} is increased. The effect of the former perturbation is dampened when Q_{II} is increased. The flow rate in zone I does not influence the extract purity.

Raffinate purity, on the other hand, is mostly affected by perturbations in Q_{III}. This flow rate controls the positioning of the leading wave of the more retained solute with respect to the raffinate port. When Q_{III} is increased, the slow-moving solute shifts past the withdrawal port and contaminates the raffinate. On the contrary, if Q_{III} is reduced then the slow solute will lag behind the raffinate port and have less chance of polluting it. Raffinate purity is also negatively affected, but to a much lesser extent, when Q_I or Q_{IV} are decreased.

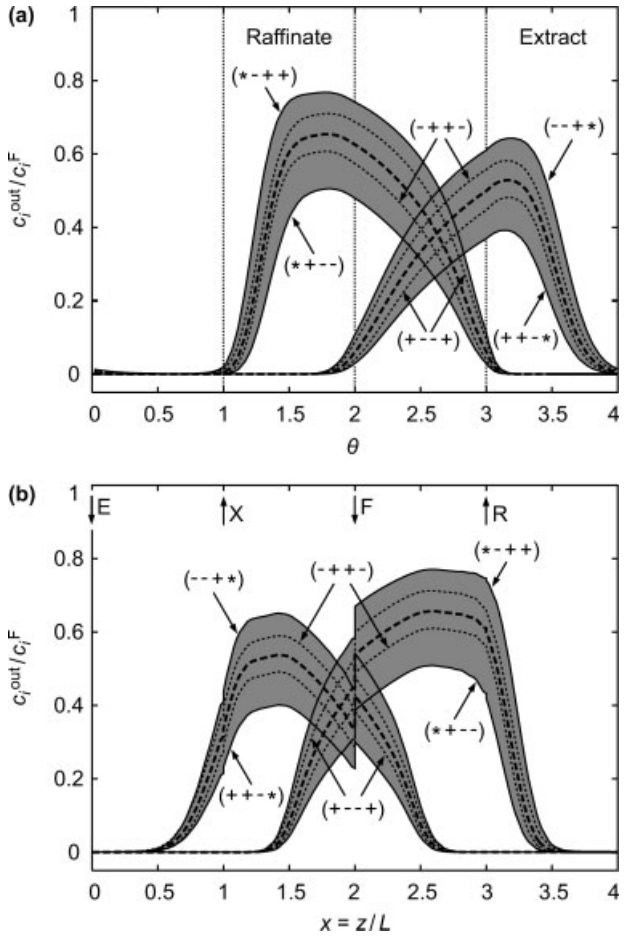

Figure 6. Steady periodic solution of the solute concentration profiles for various perturbations of the robust optimized flow rates.

The selected perturbations were taken from the factorial histograms depicted in Figure 5. The top graph (a) displays the temporal concentration profiles at a fixed column outlet, over a full CSS cycle, whereas the bottom graph (b) shows the axial concentration profiles taken at half switching interval, over the four columns. The dashed lines represent the profiles for the robust solution. Q_j^*; the dotted lines are the profiles for the two perturbations given by Eqs. 14 and 15. The gray areas show the domains of the (θ, c_i^{out}/c_i^F) and (z/L, c_i^{out}/c_i^F) planes which encompass all profiles generated by the factorial analysis. The notation ($\pm\pm\pm\pm$) stands for $(1 \pm 0.025)Q_I^*, \ldots, (1 \pm 0.025)\ Q_{IV}^*$; '*' denotes any one of $(1 - 0.025)Q_j^*$, Q_j^*, and $(1 + 0.025)Q_j^*$.

The effect of the former perturbation is less noticeable when Q_{III} is reduced. The zone II flow rate has little impact on raffinate purity.

Only 14 out of the 80 perturbed solutions satisfy both purity requirements. The purity of both products is clearly enhanced only when Q_{II} is increased, while Q_{III} is decreased, which is when the feed flow rate is reduced to the lower edge of its confidence interval. Note that the feed flow rate can be reduced via different flow rate manipulations, because it can be expressed as the difference between two zone flow rates, but not all are favorable to both extract and raffinate purities. An increase of Q_{II} enhances the extract purity, but lowers the raffinate purity unless Q_{III} is reduced to pinch the leading band of the slow-moving solute between zones III and IV. Likewise, a decrease of Q_{III} improves the raffinate purity, but degrades that of the extract unless Q_{II} is increased to prevent the trailing wave of the fast-moving solute from polluting the raffinate port.

PowerFeed operation

The optimal PowerFeed operating conditions listed in the third row of Table 2 were computed using the nominal solution for the standard SMB scheme as initial estimate. This optimization problem, consisting of 5,301 nonlinear variables, 5,280 equality constraints and 24 inequality constraints, was solved in 61.3 s and required 30 IPOPT iterations. Note that the column configuration is fixed and identical to that of the standard SMB (i.e. $N_{I,\ldots,IV} = 1$). The optimal operating conditions were subsequently rendered robust by solving the corresponding RC problem, which required 25 IPOPT iterations and was solved in 3:05 min. This RC problem has 21,141 nonlinear variables, subject to 21,120 equality constraints and 36 inequality constraints. The analysis of the residuals of g_2 revealed that the purity requirements were exactly fulfilled by the flow rate perturbations defined by Eqs. 15 and 17. If this were known beforehand, the size of the RC problem would be reduced (10,581 variables) and take only 1:31 min to solve. In any case, the present results show that even the enlarged RC problem can be solved with a modest computational effort. Note that the flow rates reported in the third and fourth rows of Table 2 are averaged values over a switching interval.

Because of the increased degrees of freedom made available when the SMB process is converted to PowerFeed operation, the nominal feed throughput is increased by 71.8% to $Q_F = 6.63$ mL/min and the solvent consumption is reduced by 49.8% to $Q_E/Q_F = 1.50$. This is a significant improvement over standard operation, but not an unexpected one if the performance gains reported in other studies are taken into consideration.[29,33,37] In agreement with the trend observed for the standard SMB scheme, the robustness in PowerFeed operation is achieved at the expense of separation performance: 27% reduction in feed throughput and 54.7% increase in solvent consumption. Note, however, that in spite of this loss in performance the robust PowerFeed scheme can still perform better than the optimized SMB scheme under nominal operating conditions.

Figure 7 compares the optimal cyclic flow rate modulations for the nominal and robust PowerFeed design problems. As expected, the zones more affected by robustness are the two ones around the active feed port. The optimal flow rate in zone I is the same regardless of the optimization problem solved, because its value is dictated by the value of Q_{max} when the productivity is maximized. For the separation and column configuration analyzed here, it is seen that when the system is rendered robust the instantaneous value of the feed flow rate is not affected, but the feed is instead injected over a smaller time interval. It is also seen that, for the robust design problem, the extract is partially obtained ahead of the feed pulse, and this is compensated by less raffinate being withdrawn over the same period. This is not the case under nominal conditions, where raffinate withdrawal is the only one which leads ahead of the feed injection.

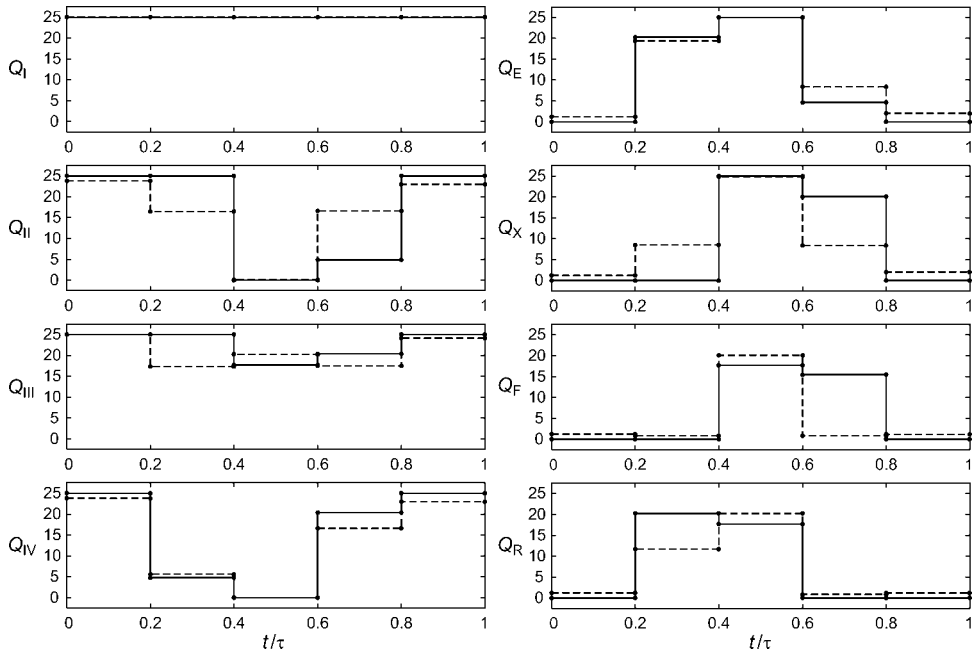

Figure 7. Optimal piecewise-constant flow rate modulation for nominal (δ = 0, solid lines) and robust (δ = 0.025, dashed lines) PowerFeed design problems.

$Q_{j=\mathrm{I},\ldots,\mathrm{IV}}$ are the zone flow rates; Q_E, Q_X, Q_F, and Q_R, denote the eluent, extract, feed, and raffinate flow rates, respectively. Flow rates are expressed in mL/min.

Varicol scheme

The optimal design problem for Varicol operation was solved using as initial estimate the nominal solution for the standard SMB scheme. From this initial guess, the port configuration and operating parameters were simultaneously optimized using the dual combination of FFSQP/IPOPT in 12.5 min. The optimization required 5 FFSQP iterations involving 23 calls to IPOPT (three of which were need for estimating the gradients of g_2 with respect to N_I, N_{II} and N_{III}, by first-order differencing). Each call to IPOPT is equivalent to solving the nominal optimization problem for a standard SMB scheme, but with less computational effort because the initial estimate for the solution is the final solution obtained in the previous call to IPOPT. The nominal Varicol operating conditions were subsequently rendered robust by solving the RC problem with FFSQP/IPOPT in 7.5 min (1 FFSQP iteration and 6 calls to IPOPT). The purity requirements were exactly fulfilled by the flow rate perturbations defined in Eqs. 14 and 16. The port configuration for the optimized Varicol scheme is 1.2/1.2/0.6/0.0, and did not change when the operating parameters were rendered robust.

The Varicol scheme gives higher productivity than the standard SMB process, and under robust conditions even surpasses that of the PowerFeed scheme, but at the expense of a higher solvent consumption. Note that zone IV is eliminated in the optimized port configuration and its flow rate modulation is close to zero for both nominal and robust solutions. As a matter of fact, Q_{IV} can be fixed at zero prior to optimizing the other decision variables with negligible impact on the final value of the objective function. Therefore, for practical purposes both nominal and robust optimized Varicol solutions are open-loop configurations in which the effluent from zone III is fully withdrawn as raffinate and none is recycled back to zone I. This is consistent with other optimization studies on linear adsorption systems.[29,33]

Note that for all three operating schemes examined in this work, the switching interval is increased by c.a. $100\delta\%$ when the nominal operating conditions are rendered robust. This is equivalent to reducing the volumetric solid flow rate of the equivalent true countercurrent process by c.a. the expected uncertainty in the zone flow rates.

Overall, the short computational times reported in this section support our claim that the proposed robust optimization procedure is computationally tractable, since a solution is generally obtained in the order of minutes. It is worth noting that this should be largely credited to IPOPT's efficient handling of a large number of variables, while exploiting the problem structure at the same time.

From the viewpoint of mathematical programming, one might argue whether it is valid to only examine the vertices of the edges that bound the 4-D flow rate uncertainty region in order to guarantee robustness, given that in principle infeasibilities may arise in nonextreme points. For the standard SMB process our claim is supported by the triangle theory.[7,8] This theory, however, is obtained from an equilibrium analysis of the true moving-bed model, which neglects finite mass-transfer resistances and assumes an infinite number of differential columns. Proving the claim using the rigorous mathematical model of the SMB process would be extremely difficult, with further increase in complexity for the Varicol and PowerFeed operating schemes.

However, our claim is strongly supported by Figure 8, which shows the results of conducting 1,000 randomly-generated perturbations of the flow rates for the nominal and

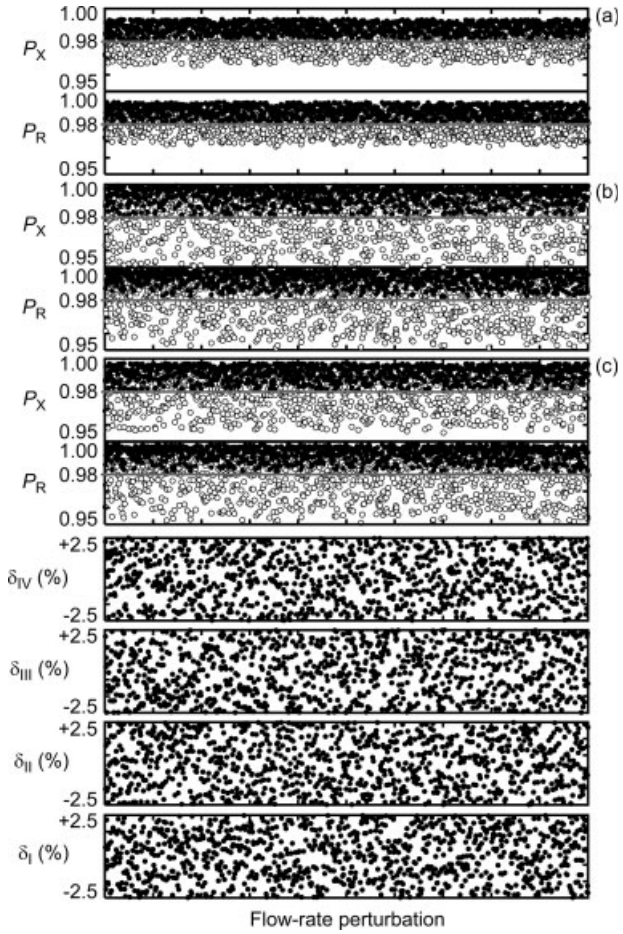

Figure 8. Extract (P_X) and raffinate (P_R) purities for 1000 randomly-generated flow rate perturbations of the robust (solid circles) and nominal (open circles) optimized solutions of the (a) standard SMB, (b) PowerFeed, and (c) Varicol schemes.

The obtained purity ranges, [P_R^{min}, P_R^{max}; P_X^{min}, P_X^{max}], for the perturbed nominal solutions are [0.967, 0.988; 0.965, 0.988] (SMB), [0.951, 0.995; 0.950, 0.996] (PowerFeed), and [0.950, 0.994; 0.955, 0.992] (Varicol); those for the robust solutions are [0.981, 0.994; 0.981, 0.994] (SMB), [0.982, 0.999; 0.981, 0.999] (PowerFeed), and [0.981, 0.998; 0.981, 0.997] (Varicol).

robust solutions listed in Table 2 within the specified uncertainty interval of $\pm 2.5\%$. The four bottom graphs are scatter plots of the perturbed flow rates, showing that the uncertainty region in the internal flow rates was uniformly probed over its full extent. Each of the three graphs at the top of Figure 8 compares the raffinate and extract purities for the 1,000 perturbations of the nominal and robust solutions of a given operating scheme. It is clearly shown that the raffinate and extract purities for the perturbations of the robust solutions are all kept above 98%, whereas those for the nominal solutions are in many cases below 98%; in the worst cases the purities drop to 95%. It is also interesting to notice that the purities for the perturbations of the standard SMB scheme vary over a tighter range than those of the PowerFeed and Varicol schemes. This shows that the enhanced process performance provided by these two schemes is subjected to an increased sensitivity to operating disturbances. The numerical experiments reported here have been repeated for several solution points along the Pareto curves discussed in the next section, and in every case the random perturbations of the robust solutions remained feasible. Thus, there is strong evidence that the worst-case perturbations are among the vertices of the 4-D flow-rate uncertainty region.

Multiobjective optimization

In the more general case, optimal SMB design is a two-objective optimization problem, in which productivity is to be maximized and eluent consumption is to be minimized, subject to the h and g sets of constraints, that is

$$\max_{\tau, N_j, Q_j^*} \overline{Q}_F^* \tag{23}$$

$$\min_{\tau, N_j, Q_j^*} \overline{Q}_E^* \tag{24}$$

$$\text{s.t. } y = h^{CSS}(\tau, N_j, Q_j^*) \tag{25}$$

$$g(\tau, N_j, Q_j^*, y) \geq 0 \tag{26}$$

Using the aforementioned formulation, robust values of the decision variables can be determined for progressively larger values of solvent consumption Q_E^{max}, by converting the second objective function into an extra inequality constraint, i.e.

$$\overline{Q}_E^* \leq Q_E^{max} \tag{27}$$

and, possibly, by also eliminating the constraints on the maximum allowed internal flow rates. This gives rise to a robust Pareto set. The mathematical theory of Pareto multiobjective optimization is somewhat complex,[38,39] but some basic definitions and properties are easily explained for the special case of dual-objective. In this case, each Pareto curve represents the opposing objectives of maximizing productivity, and minimizing solvent consumption for a given number of columns and operating scheme.

Figure 9 shows nominal and robust Pareto optimal solutions for the SMB, Varicol and PowerFeed operating schemes. The *-labels denote the robust Pareto curves for a $\pm 2.5\%$ flow rate uncertainty. Any point above the Pareto curve has worse performance than the points constituting the Pareto curve, because there is always one element of the Pareto set which has a lower solvent consumption for the same productivity. The points located below the Pareto curve are not feasible because the purity requirements are not fulfilled. When moving along the Pareto curve, each point is nondominant with respect to the others. The choice of a particular point in the Pareto curve over all other points requires additional considerations about the problem, such as the overall separation cost and profit functions, which are outside the scope of the present work. Note that the Pareto curves exist only in finite domains of the Q_E/Q_F-vs-Q_F plane and that the extent of the domain enclosing a given Pareto curve is a measure of versatility of the corresponding operating scheme.[40] For convenience, only the nominal and robust Par-

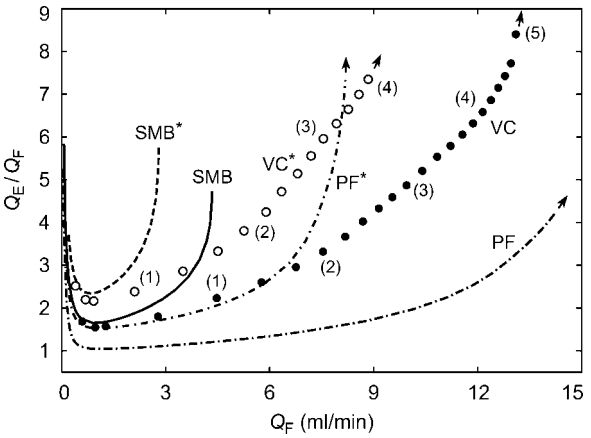

Figure 9. Pareto optimal solutions for standard (SMB), Varicol (VC) and PowerFeed (PF) operating schemes.

The *-labels denote the robust Pareto curves for a ±2.5% flow rate uncertainty. An arrow indicates that the full curve extends to higher productivities than what is plotted. Some optimized port configurations for the nominal Varicol schemes are (1) 0.8/1.2/1.2/0.8, (2) 0.8/1.2/1.4/0.6, (3) 0.7/1.3/1.4/0.6, (4) 1.0/1.3/1.7/0.0, (5) 1.0/1.4/1.6/0.0, and for the robust counterparts are (1) 0.9/1.2/1.2/0.7, (2) 0.8/1.2/1.4/0.6, (3) 1.0/1.3/1.7/0.0, (4) 1.0/1.4/1.6/0.0.

eto curves for the standard SMB scheme are fully plotted in Figure 9.

Overall, the results show that PowerFeed is the best operating scheme because it not only exhibits the lowest Pareto curve but also the one with the widest extent, i.e. its specific eluent consumption is consistently lower than those of the other two schemes, and the system with-stands higher feed throughputs without violating the purity constraints. The Varicol scheme also clearly outperforms the standard SMB process, both in productivity and eluent consumption, but it is not as efficient as the PowerFeed scheme for the separation under study. When both schemes are operated under robust conditions, however, the Varicol process outperforms the PowerFeed scheme in the upper end of the feed throughput region. The reason for this is discussed later.

For very low-feed throughputs the SMB and Varicol processes are nearly coincident; in fact, the optimized Varicol port configuration tends to 1/1/1/1 as the feed flow rate is decreased towards zero. This is in agreement with previous studies.[29,32,33] However, as the feed flow rate is increased the optimized Varicol column configuration increases the length of zones II and III at the expense of that of zone IV, which is eliminated altogether for the highest feed throughputs.

It is worth noting that for all three operating schemes, process performance degrades significantly for very small values of Q_F. This is due to the explicit modeling of extra volumes in the system as perfectly mixed cells placed between every two adjacent columns. When the system is operated at a very low flow rate, the residence time in the mixing cells, V_e/Q_j, is of the same order of magnitude or larger than the residence time in a column, $(1 + \beta K_i)L/v$. The same net effect is likely to be observed if the complete van Deemter curve, incorporating a term proportional to $1/v$, is employed. If band broadening is exclusively taken into account through a linear van Deemter curve, as in Eq. 21, it can be shown that the Q_E/Q_F-vs-Q_F Pareto curve is a monotonically increasing function of Q_F.[32,33]

Figure 9 shows that for all three schemes, the robust Pareto curve shifts upwards and the extent of the domain enclosing it diminishes with respect to its nominal counterpart. This shows that robustness is achieved at the expense of a higher eluent consumption and/or lower feed throughput over the whole operating range. Differences between nominal and robust process performances for the three operating schemes are more apparent in the higher feed-throughput region. This is particularly noticeable for PowerFeed operation. This is not surprising, given that the performance of this scheme is entirely dependent on flow rate manipulation.

The performance penalty when switching from nominal to robust operation is best perceived in Figure 10, in which the ratio of robust to nominal feed throughputs, $Q_F(\delta = 2.5\%)/Q_F(\delta = 0\%)$, is plotted as a function of eluent flow rate for each operating scheme. Note that the selection of Q_E as independent variable is only a matter of convenience to expand the scale on the x-axis; the same trends would be observed if Q_F were selected instead.

The curves for the standard SMB process and PowerFeed scheme exhibit a maximum for $Q_E \approx 4$ mL/min, where robust operation is the least detrimental on productivity with respect to its nominal counterpart. At higher flow rates, the performance penalty for operating under robust conditions increases more or less linearly with Q_E. Notice also that over most of the operating range, the standard SMB process is somewhat less sensitive to robustness than the PowerFeed scheme.

The Varicol process exhibits an entirely different behavior from the other two schemes. The robust-to-nominal productivity ratio for the Varicol scheme increases steadily with Q_E up to $Q_E \approx 10$ mL/min, and remains constant at a value of about 0.79 for higher values of Q_E. Thus, as opposed to the other two schemes, Varicol productivity is less affected at higher flow rates than at lower ones when its operating parameters are rendered robust. This is partly due to its trend towards a three-zone open-loop configuration, and, hence, reduced sensitivity to perturbations in Q_{IV}, as the feed flow rate is increased.

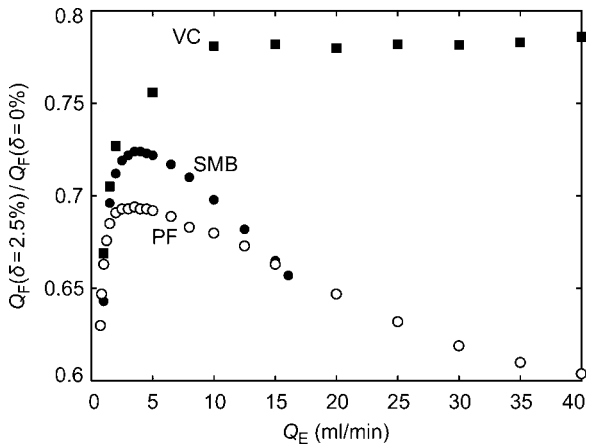

Figure 10. Robust-to-nominal productivity ratio, $Q_F(\delta = 2.5\%)/Q_F(\delta = 0\%)$, as a function of eluent flow rate for standard (SMB), Varicol (VC), and PowerFeed (PF) operating schemes.

Figure 9 also shows that the smallest performance penalty incurred by robust operation is for the Varicol scheme, whereas the largest one is for PowerFeed operation. Overall, however, Figure 9 shows that PowerFeed operation remains the most efficient scheme for the separation under study, except near the upper limit of the robust feed throughput-region, where Varicol performs better. It has recently been shown[29,32,33,37] that the combination of Varicol and PowerFeed schemes into a single hybrid process provides further performance enhancements with respect to the individual schemes. This is particularly apparent for compact units with a small number of columns. The present results suggest that asynchronous port switching may significantly improve the performance of flow-rate modulation under robust conditions. This, however, will not be presently explored, since it deserves a more detailed study in a separate publication.

Conclusions

A general procedure for robust design of SMB processes under flow rate uncertainty was developed in the frame of rigorous optimization theory. The best solution is chosen only among candidate solutions that are robust feasible, that is, remain feasible for all flow rate perturbations from the uncertainty set. Computational tractability is ensured by formulating the robust problem with only the vertices of the uncertainty domain that most adversely affect the raffinate and extract purities. In practice, the nominal problem is replaced by a worst case problem.

The procedure was successfully employed to find robust operating conditions for the linear separation of two nucleosides by standard SMB, Varicol, and PowerFeed schemes. The pros and cons of running each scheme under nominal and robust operating conditions were discussed. Regardless of the operating mode, robustness is achieved at the expense of a higher eluent consumption and/or lower feed throughput. Furthermore, differences between nominal and robust process performances are more apparent in the higher feed-throughput region, except for the Varicol scheme which shows the opposite trend. PowerFeed operation was found to be the most efficient operating scheme for the separation under study, although Varicol was also seen to clearly outperform the standard SMB process. However, it was also shown that Varicol productivity is the least less affected by robustness, whereas that of PowerFeed is the most affected.

In future work, our method will be employed to find robust operating conditions for nonlinear separations, and to analyze the influence of isotherm shape and feed concentration on performance parameters, such as the robust-to-nominal productivity ratio, for the different operating schemes considered here.

Acknowledgments

Support from FCT/MCES (Portugal), through project POCTI/EQU/39391/2001 and PhD grants (SFRH/BD) 13721/2003 and 19267/2004, is gratefully acknowledged.

Notation

c = solute concentration, g/l
H = plate height, cm
L = column length, cm
mod = modulo operator, $a \bmod b = a - b\ \mathrm{int}(a/b)$
N = number of columns
Pe = Péclet number
q = adsorbed concentration, g/l
Q = flow rate, cm^3/min
t = time, min
v = linear velocity, cm/min
V_e = extra-column volume, cm^3
z = axial position in column, cm

Greek letters

β = phase ratio, $(1 - \varepsilon)/\varepsilon$
ε = interparticle porosity
τ = switching interval, min
θ = dimensionless time, t/τ
$\theta' = \theta \bmod 1$
$\bar{\theta} = \theta \bmod N$

Subscripts and superscripts

E = eluent
F = feed
i = solute index
I,. . .,IV = zone index
in = inlet effluent
j = column index
out = outlet effluent
R = raffinate
X = extract

Literature Cited

1. Strube J, Haumreisser S, Schmidt-Traub H, Schulte M, Ditz R. Comparison of batch elution chromatography and continuous simulated moving bed chromatography. *Org Process Res Dev*. 1998; 2:305–319.
2. Miller L, Grill C, Yan T, Dapremont O, Juza M. Batch and simulated moving bed chromatographic resolution of a pharmaceutical racemate. *J Chromatogr A*. 2003;1006:267.
3. Grill CM, Miller L, Yan TQ. Resolution of a racemic pharmaceutical intermediate: A comparison of preparative HPLC, steady state recycling, and simulated moving bed. *J Chromatogr A*. 2004; 1026:101.
4. Ruthven DM, Ching CB. Countercurrent and simulated countercurrent adsorption separation processes. *Chem Eng Sci*. 1989;44:1011.
5. Chin CY, Wang N-HL. Simulated moving bed equipment designs. *Sep Purif Rev*. 2004;33:77.
6. Juza M, Mazzotti M, Morbidelli M. Simulated moving bed chromatography and its applications to chiraltechnology. *Trends Biotech*. 2000;18:108.
7. Storti G, Mazzotti M, Morbidelli M, Carrà A. Robust design of binary countercurrent adsorption separation processes. *AIChE J*. 1993;39:471.
8. Mazzotti M, Storti G, Morbidelli M. Optimal operation of simulated moving bed units for nonlinear chromatographic separations. *J Chromatogr A*. 1997;769:3–24.
9. Mun S, Xie Y, Wang N-HL. Robust pinched-wave design of a size-exclusion simulated moving-bed process for insulin purification. *Ind Eng Chem Res*. 2003;42:3129.
10. Ma Z, Wang N-HL. Standing wave analysis of SMB chromatography: Linear systems. *AIChE J*. 1997;43:2488.
11. Hritzko BJ, Xie Y, Wooley RJ, Wang N-HL. Standing wave design of tandem SMB for linear multicomponent systems. *AIChE J*. 2002; 48:2769.
12. Adam P, Nicoud RM, Bailly M, Ludemann-Hombourger O. Process and device for separation with variable-length. US Patent 6,136,198, 2000.
13. Ludemann-Hombourger O, Nicoud RM, Bailly M. The Varicol process: a new multicolumn continuous chromatographic process. *Sep Sci Technol*. 2000;35:1829.
14. Kearney MM, Hieb KL. Time variable simulated moving bed process. US Patent 5,102,553, 1992.

15. Kloppenburg E, Gilles ED. A new concept for operating simulated moving-bed processes. *Chem Eng Technol*. 1999;22:313.
16. Zang Y, Wankat PC. SMB operation strategy-Partial feed. *Ind Eng Chem Res*. 2002;41:2504.
17. Zhang Z, Mazzotti M, Morbidelli M. PowerFeed operation of simulated moving bed units: changing flow-rates during a switching interval. *J Chromatogr A*. 2003;1006:87.
18. Zhang Z, Mazzotti M, Morbidelli M. Experimental assessment of PowerFeed chromatography. *AIChE J*. 2004;50:625.
19. Grossmann, IE, Sargent, RWH. Optimum design of chemical plants with uncertain parameters. *AIChE J*. 1978;24:1021.
20. Halemane, KP, Grossmann, IE. Optimal process design under uncertainty. *AIChE J*. 1983;29:425.
21. Biegler LT, Grossmann, IE, Westerberg, AW. *Systematic Methods of Chemical Process Design*. Chap. 21. Englewood Cliffs, NJ: Prentice Hall; 1997.
22. Ben-Tal A, Nemisovski A. Robust optimization—Methodology and applications. *Math Program Ser B*. 2002;92:453.
23. Araújo JMM, Rodrigues RCR, Mota JPB. Optimal design and operation of a certain class of asynchronous simulated moving bed processes. *J. Chromatogr A*. 2006;1132:76.
24. Toumi A, Hanisch F, Engell S. Optimal operation of continuous chromatographic processes: Mathematical optimization of the varicol process. *Ind Eng Chem Res*. 2002;41:4328.
25. Toumi A, Engell S, Ludemann-Hombourger O, Nicoud RM, Bailly M. Optimization of simulated moving bed and varicol processes. *J. Chromatogr A*. 2003;1006:15.
26. Mota JPB, Araújo JMM. Single-column simulated moving-bed with recycle lag. *AIChE J*. 2005;51:1641–1653.
27. Araújo JMM, Rodrigues RCR, Mota JPB. Use of single-column models for efficient computation of the periodic state of a simulated moving-bed process. *Ind Eng Chem Res*. 2006;45:5314.
28. Kawajiri Y, Biegler LT. Optimization strategies for simulated moving bed and Powerfeed processes. *AIChE J*. 2006;52:1343.
29. Kawajiri Y, Biegler LT. Nonlinear programming superstructure for optimal dynamic operations of simulated moving bed processes. *Ind Eng Chem Res*. 2006;45:8503.
30. Fourer R, Gay DM, Kernighan BW. *AMPL - A Modeling Language for Mathematical Programming*, 2nd ed. CA: Brooks/Cole Thomson Learning; 2003.
31. Wachter A, Biegler LT. On the implementation of an interior point filter line search algorithm for large-scale nonlinear progamming. *Math Prog*. 2005;106:25.
32. Rodrigues RCR, Araújo JMM, Eusébio MFJ, Mota JPB. Experimental assessment of simulated moving bed and varicol processes using a single-column setup. *J Chromatogr A*. 2006;1142:69.
33. Rodrigues RCR, Araújo JMM, Eusébio MFJ, Mota JPB. Optimal design and experimental validation of synchronous, asynchronous and flow-modulated, simulated moving bed processes using a single-column setup. *J Chromatogr A*. 2007; doi:10.1016/j.chroma.2007.01.103.
34. Mota JPB, Esteves IAAC, Eusébio MFJ. Synchronous and asynchronous SMB processes for gas separation. *AIChE J*. 2007;53:1192.
35. Zhou JL, Tits AL, Lawrence CT. *User's Guide for FFSQP Version 3.7*. Tucker, GA: AEM Design Inc.; 1998.
36. Abel S, Erdem G, Amanullah M, Morari M, Mazzotti M, Morbidelli M. Optimizing control of simulated moving bed—experimental implementation. *J Chromatogr A*. 2005;1092:2.
37. Zhang Z, Mazzotti M, Morbidelli M. Continuous chromatographic processes with a small number of columns: comparison of simulated moving bed with varicol, powerfeed and modicon. *Korean J Chem Eng*. 2004;21:454.
38. Miettinen K. *Nonlinear Multiobjective Optimisation*. Dordrecht, The Netherlands: Kluwen; 1999.
39. Deb K. *Multi-objective Optimization Using Evolutionary Algorithms*. Chichester: Wiley; 2001.
40. Paredes G, Mazzotti M. Optimization of simulated moving bed and column chromatography for a plasmid DNA purification step and for a chiral separation. *J Chromatogr A*. 2006; doi:10.1016/j.chroma.2006.12.009

Manuscript received Mar. 13, 2007, revision received May 31, 2007, and final revision received July 17, 2007.